Inorg. Chem. **2008**, *47*, 2368−2379

Structural Characterization, Solution Studies, and DFT Calculations on a Series of Binuclear Gold(III) Oxo Complexes: Relationships to Biological Properties

Chiara Gabbiani,[†] Angela Casini,[†] Luigi Messori,[*,†] Annalisa Guerri,[‡] Maria Agostina Cinellu,[*,§] Giovanni Minghetti,[§] Maddalena Corsini,[||] Claudia Rosani,[||] Piero Zanello,[||] and Massimiliano Arca[⊥]

Dipartimento di Chimica and CRIST, Centro Interdipartimentale di Cristallografia Strutturale, Università di Firenze, Polo Scientifico, Via della Lastruccia 3, 50019 Sesto Fiorentino, Firenze, Italy, Dipartimento di Chimica, Università di Sassari, Via Vienna 2, 07100 Sassari, Italy, Dipartmento di Chimica, Università di Siena, Via A. Moro, 53100 Siena, Italy, and Dipartimento di Chimica Inorganica ed Analitica, Università degli Studi di Cagliari, S.S. 554 bivio per Sestu, 09042 Monserrato (CA), Italy

Received June 26, 2007

A series of structurally related oxo-bridged binuclear gold(III) compounds, $[Au_2(\mu\text{-}O)_2(N\text{^}N)_2](PF_6)_2$, where N^N is 2,2′-bipyridine or a substituted 2,2′-bipyridine, have recently been shown to exhibit appreciable stability under physiological-like conditions and to manifest important antiproliferative effects toward selected human tumor cell lines (*J. Med. Chem.* **2006**, *49*, 5524). The crystal structures of four members of this series, namely, $[Au_2(\mu\text{-}O)_2(bipy)_2](PF_6)_2$, *cis*-$[Au_2(\mu\text{-}O)_2(6\text{-}Mebipy)_2](PF_6)_2$, *trans*-$[Au_2(\mu\text{-}O)_2(6\text{-}oXylbipy)_2](PF_6)_2$, and $[Au_2(\mu\text{-}O)_2(6,6'\text{-}Me_2bipy)_2](PF_6)_2$, have been solved here and the respective structural parameters comparatively analyzed. Remarkably, all of the compounds contain a common structural motif consisting of a Au_2O_2 "diamond core" linked to two bipyridine ligands in a roughly planar arrangement. Interestingly, introduction of different kinds of alkyl or aryl substituents on the 6 (and 6′) position(s) of the bipyridine ligand leads to small structural changes that nonetheless greatly affect the reactivity of the metal centers. The chemical behavior of these compounds in solution has been studied in detail, focusing in particular on the electrochemical properties. Some initial correlations among the structural parameters, the chemical behavior in solution, and the known cytotoxic effects of these compounds are proposed. Notably, we have found that the 6,6′-dimethyl-2,2′-bipyridine derivative, which showed the largest structural deviations with respect to the model compound $[Au_2(\mu\text{-}O)_2(bipy)_2](PF_6)_2$, also had the highest oxidizing power, the least thermal stability, and the greatest cytotoxic activity. The positive correlation that exists between the oxidizing power and the antiproliferative effects seems to be of particular interest. Moreover, the electronic structures of these compounds were extensively analyzed using DFT methods, and the effects of the various substituents on reactivity were predicted; overall, very good agreement between theoretical expectations and experimental data was achieved. In turn, theoretical predictions offer interesting hints for the design of new, more active binuclear gold(III) compounds.

Introduction

In recent years, great interest has been focused on gold(III) complexes as cytotoxic and antitumor drugs.[1] The renaissance of interest in gold(III) complexes as potential anticancer agents started in the 1990s, when Buckley, Parish, and co-workers described a new series of cyclometalated gold(III) complexes of the type $[Au(N\text{^}C)X_2]$ (N^C = *o*-$C_6H_4CH_2NMe_2$; X = monodentate anionic ligand or X_2 = bidentate dianionic ligand), which exhibit appreciable chemical stability and significant cytotoxic and antitumor properties.[2] Subsequently, a number of cycloaurated derivatives containing bidentate ligands $\{[Au(N\text{^}C)X_2]^{3-6}\}$ or tridentate ligands $\{[Au(N\text{^}N\text{^}C)X]^+$ [N^N^CH = 6-(1,1-dimethylbenzyl)-2,2′-bipyridine; X = OH, NHAr][6,7] and

* To whom correspondence should be addressed. E-mail, luigi.messori@unifi.it; phone, +39 055 4573388; fax, +39 055 4573385 (L.M.). E-mail, cinellu@uniss.it; phone, +39 079 229499; fax, +39 079 229559 (M.A.C.).
† Dipartimento di Chimica, Università di Firenze.
‡ CRIST, Centro Interdipartimentale di Cristallografia Strutturale, Università di Firenze.
§ Università di Sassari.
|| Università di Siena.
⊥ Università degli Studi di Cagliari.

10.1021/ic701254s CCC: $40.75
Published on Web 03/04/2008

Chart 1. 2,2′-Bipyridine-Based Ligands N^N and Gold(III) Oxo Complexes $[Au_2(\mu\text{-}O)_2(N\text{^}N)_2](PF_6)_2$ (**1**−**6**)[a]

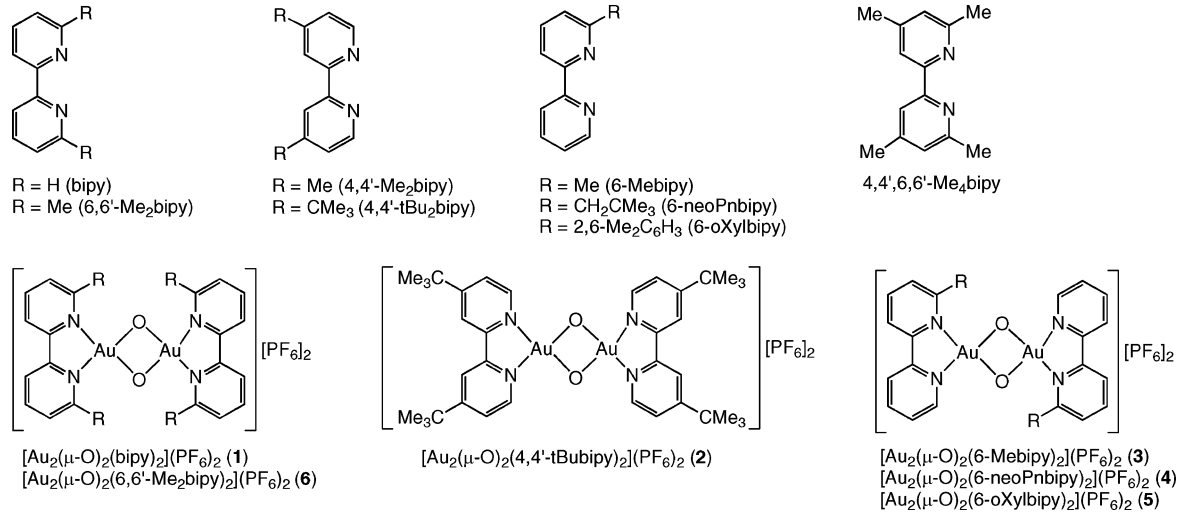

[a] Complex **3** was obtained as an ∼1:1 mixture of the cis and trans isomers, while **4** and **5** were obtained as the pure trans isomers, as depicted.

$[Au_m(C\text{^}N\text{^}C)_mL]^{n+}$ (HC^N^CH = 2,6-diphenylpyridine; L = N or P donor; m = 1–3; n = 0–3)[8]} were characterized and shown to exert relevant cytotoxic effects on human carcinoma xenografts. In addition to these organometallic compounds, a variety of gold(III) complexes with multidentate chelating ligands, such as polyamines,[9] polypyridines,[7,9b–d,10] phenanthrolines,[9b–d] porphyrins,[11] and dithiocarbamates,[12] were found to be fairly stable against reduction to metallic gold under physiological-like conditions and to display promising tumor-cell killing properties as well.

We recently reported our studies of a series of six oxo-bridged binuclear gold(III) complexes $[Au_2(\mu\text{-}O)_2(N\text{^}N)_2](PF_6)_2$(**1**−**6**), where N^N = 2,2′-bipyridine (bipy) in **1**; 4,4′-di-*tert*-butyl-2,2′-bipyridine (4,4′-tBu_2bipy) in **2**; 6-methyl-2,2′-bipyridine (6-Mebipy) in **3**; 6-neopentyl-2,2′-bipyridine (6-neoPenbipy) in **4**; 6-(2,6-dimethylphenyl)-2,2′-bipyridine (6-oXylbipy) in **5**; and 6,6′-dimethyl-2,2′-bipyridine (6,6′-Me_2bipy) in **6** (see Chart 1).[13] These compounds displayed favorable stability profiles in buffered aqueous solutions and manifested significant cytotoxic properties in vitro. Notably, rather large differences among the investigated complexes in terms of relative cytotoxic potency emerged, as shown, for example, by the IC_{50} values against the A2780/S cell line, which ranged from 25.4 to 1.79 μM.[13] In particular, compound **6**, containing the 6,6′-dimethyl-2,2′-bipyridine ligand, turned out to manifest far stronger antiproliferative properties than the other members of this series. As differences in cytotoxicity were evidently correlated to the nature of the 2,2′-bipyridine ligand, we started a more extensive investigation

(1) (a) Messori, L.; Marcon, G. *Met. Ions Biol. Syst.* **2004**, *42*, 385. (b) Shaw, C. F., III *Chem. Rev.* **1999**, *99*, 2589. (c) Tiekink, E. R. *Crit. Rev. Oncol. Hematol.* **2002**, *42*, 225.

(2) (a) Parish, R. V.; Howe, B. P.; Wright, J. P.; Mack, J.; Pritchard, R. G.; Buckley, R. G.; Elsome, A. M.; Fricker, S. P. *Inorg. Chem.* **1996**, *35*, 1659. (b) Parish, R. V.; Mack, J.; Hargreaves, L.; Wright, J. P.; Buckley, R. G.; Elsome, A. M.; Fricker, S. P.; Theobald, B. R. C. *J. Chem. Soc., Dalton Trans.* **1996**, 69. (c) Buckley, R. G.; Elsome, A. M.; Fricker, S. P.; Henderson, G. R.; Theobald, B. R. C.; Parish, R. V.; Howe, B. P.; Kelland, L. R. *J. Med. Chem.* **1996**, *39*, 5208.

(3) C^N = $C_6H_3(CH_2NMe_2)$-2-(OMe)-5, H_2X_2 = *N*,*N*′-diacetylurea or thiosalicylic acid: (a) Dinger, M. B.; Henderson, W. *J. Organomet. Chem.* **1998**, *557*, 231. (b) Dinger, M. B.; Henderson, W. *J. Organomet. Chem.* **1998**, *560*, 233.

(4) HC^N = 2-arylpyridine, 2-anilinopyridine, or 2-benzylpyridine; X_2 = thiosalicylate, catecholate, $CHRSO_2CHR$, or bis(amidate) ligands: (a) Henderson, H.; Nicholson, B. K.; Faville, S. J.; Fan, D.; Ranford, J. D. *J. Organomet. Chem.* **2001**, *631*, 41. (b) Goss, C. H. A.; Henderson, W.; Wilkins, A. L.; Evans, C. *J. Organomet. Chem.* **2003**, *679*, 194. (c) Henderson, W.; Nicholson, B. K.; Wilkins, A. L. *J. Organomet. Chem.* **2005**, *690*, 4971. (d) Kilpin, K. J.; Henderson, W.; Nicholson, B. K. *Polyhedron* **2007**, *26*, 434.

(5) HC^N = 2-phenylpyridine, X = carboxylate or thiolate ligands, or X_2 = dicarboxylate or bidentate thiolate ligands:(a) Fan, D.; Yang, C.-T.; Ranford, J. D.; Lee, P. F.; Vittal, J. J. *Dalton Trans.* **2003**, 2680. (b) Fan, D.; Yang, C.-T.; Ranford, J. D.; Vittal, J. J.; Lee, P. F. *Dalton Trans.* **2003**, 3376.

(6) HC^N = 2-(1,1-dimethylbenzyl)pyridine, X = AcO:(a) Messori, L.; Marcon, G.; Cinellu, M. A.; Coronnello, M.; Mini, E.; Gabbiani, C.; Orioli, P. *Bioorg. Med. Chem.* **2004**, *12*, 6039. (b) Rigobello, M. P.; Messori, L.; Marcon, G.; Cinellu, M. A.; Bragadin, M.; Folda, A.; Scutari, G.; Bindoli, A. *J. Inorg. Biochem.* **2004**, *98*, 1634. (c) Coronnello, M.; Mini, E.; Caciagli, B.; Cinellu, M. A.; Bindoli, A.; Gabbiani, C.; Messori, L. *J. Med. Chem.* **2005**, *48*, 6761.

(7) Marcon, G.; Carotti, S.; Coronnello, M.; Messori, L.; Mini, E.; Orioli, P.; Mazzei, T.; Cinellu, M. A.; Minghetti, G. *J. Med. Chem.* **2002**, *45*, 1672.

(8) Li, C. K.-L.; Sun, R. W.-Y.; Kui, S. C.-F.; Zhu, N.; Che, C.-M. *Chem.—Eur. J.* **2006**, *12*, 5253.

(9) (a) Carotti, S.; Guerri, A.; Mazzei, T.; Messori, L.; Mini, E.; Orioli, P. *Inorg. Chim. Acta* **1998**, *281*, 90. (b) Messori, L.; Abbatte, F.; Marcon, G.; Orioli, P.; Fontani, M.; Mini, E.; Mazzei, T.; Carotti, S.; O'Connell, T.; Zanello, P. *J. Med. Chem.* **2000**, *43*, 3541. (c) Messori, L.; Marcon, G.; Tempi, C.; Orioli, P. *Biochem. Biophys. Res. Commun.* **2001**, *281*, 352. (d) Coronnello, M.; Marcon, G.; Carotti, S.; Caciagli, B.; Mazzei, T.; Mini, E.; Orioli, P.; Messori, L. *Oncol. Res.* **2001**, *12*, 361.

(10) Palanichamy, K.; Ontko, A. C. *Inorg. Chim. Acta* **2006**, *359*, 44.

(11) (a) Che, C.-M.; Sun, R. W.-Y.; Yu, W.-Y.; Ko, C.-B.; Zhu, N.; Sun, H. *Chem. Commun.* **2003**, 1718. (b) Wang, Y.; He, Q.-Y.; Sun, R. W.-Y.; Che, C.-M.; Chiu, J.-F. *Cancer Res.* **2005**, *65*, 11553. (c) Wang, Y.; He, Q.-Y.; Che, C.-M.; Chiu, J.-F. *Proteomics* **2006**, *6*, 131. (d) Lum, C. T.; Yang, Z. F.; Li, H. Y.; Sun, R. W.-Y.; Fan, S. T.; Poon, R. T. P.; Lin, M. C. M.; Che, C.-M.; Kung, H. F. *Int. J. Cancer* **2006**, *118*, 1527. (e) Wang, Y.; He, Q.-Y.; Sun, R. W.-Y.; Che, C.-M.; Chiu, J.-F. *Eur. J. Pharmacol.* **2007**, *554*, 113.

(12) (a) Ronconi, L.; Giovagnini, L.; Marzano, C.; Bettio, F.; Graziani, R.; Pilloni, G.; Fregona, D. *Inorg. Chem.* **2005**, *44*, 1867. (b) Giovagnini, L.; Ronconi, L.; Aldinucci, D.; Lorenzon, D.; Sitran, S.; Fregona, D. *J. Med. Chem.* **2005**, *48*, 1588.

(13) Casini, A.; Cinellu, M. A.; Minghetti, G.; Gabbiani, C.; Coronnello, M.; Mini, E.; Messori, L. *J. Med. Chem.* **2006**, *49*, 5524.

Table 1. Crystallographic Data and Refinement Parameters for Compounds **1**, *cis*-**3**, *trans*-**5**, and **6**

parameter	**1**·2CH$_3$CN	*cis*-**3**·CH$_3$CN	*trans*-**5**·2CH$_3$CN	**6**
empirical formula	$C_{24}H_{20}Au_2F_{12}N_6O_2P_2$	$C_{24}H_{23}Au_2F_{12}N_5O_2P_2$	$C_{40}H_{38}Au_2F_{12}N_6O_2P_2$	$C_{24}H_{24}Au_2F_{12}N_4O_2P_2$
formula weight	1108.33	1097.35	1318.64	1084.34
temperature (K)	298	298	298	298
wavelength (Å)	0.7107	0.7107	0.7107	0.7107
crystal system, space group	triclinic, $P\bar{1}$	monoclinic, $P2_1/c$	monoclinic, $P2_1/n$	monoclinic, $C2/m$
unit cell parameters				
a (Å)	7.1943(9)	8.8396(7)	12.0820(10)	14.687(3)
b (Å)	11.212(1)	17.472(2)	14.946(2)	13.241(2)
c (Å)	11.346(1)	20.235(2)	12.378(1)	7.639(2)
α (deg)	63.10(1)			
β (deg)	86.00(1)	99.108(7)	97.528(9)	95.30(2)
γ (deg)	81.98(1)			
volume (Å^3)	808.2(1)	3085.8(5)	2215.9(4)	1479.2(5)
Z, D_c (mg/cm^3)	1, 2.277	4, 2.362	2, 1.976	2, 2.435
μ (mm^{-1})	9.269	9.708	6.779	10.123
F(000)	518	2056	1264	1016
R indices R1, wR2[a]				
final [$I > 2\sigma(I)$]	0.0425, 0.1096	0.0456, 0.0898	0.0479, 0.1154	0.0411, 0.0944
all data	0.0532, 0.1173	0.0902, 0.1022	0.0833, 0.1296	0.0451, 0.0982

[a] $R1 = \sum||F_o| - |F_c||/\sum|F_o|$; $wR2 = \{\sum[w(F_o^2 - F_c^2)^2]/\sum[w(F_o^2)^2]\}^{1/2}$.

of the structural and solution chemistry of these compounds in order to elucidate the possible chemical reasons for their biological properties.

Here we describe the crystal structures of [Au$_2$(μ-O)$_2$(bipy)$_2$](PF$_6$)$_2$ (**1**), *cis*-[Au$_2$(μ-O)$_2$(6-Mebipy)$_2$](PF$_6$)$_2$ (*cis*-**3**), *trans*-[Au$_2$(μ-O)$_2$(6-oXylbipy)$_2$](PF$_6$)$_2$ (*trans*-**5**), and [Au$_2$(μ-O)$_2$(6,6′-Me$_2$bipy)$_2$](PF$_6$)$_2$ (**6**); structural data for *trans*-[Au$_2$(μ-O)$_2$(6-neoPenbipy)$_2$](PF$_6$)$_2$ (*trans*-**4**)[14] are also analyzed for the sake of comparison. Using **1** as a reference compound, we conducted an in-depth examination of the alterations that the bipyridine substituents induced in the structural parameters of the various complexes.

The solution behavior of all six compounds was monitored by electronic absorption spectroscopy, focusing in particular on a comparative analysis of their thermal stability profiles. In addition, classical electrochemical methods were applied in order to define their respective electron-transfer abilities. Finally, detailed density functional theory (DFT) calculations were performed to further substantiate and better interpret the great amount of experimental data obtained.

Overall, the main goal of the present study was the identification of possible structure–function relationships that might link the chemical and structural properties of the compounds to their known biological effects and, hopefully, explain their peculiar pattern. Moreover, thanks to the application of DFT methods, we have tried to provide a solid theoretical background for the experimental results. On the whole, this kind of information may prove to be crucial for the design of new, more active polymetallic gold(III) compounds that can be further developed as cytotoxic and antitumor agents.

Experimental Section

Synthesis of the Gold(III) Oxo Complexes. The title compounds **1–6** were synthesized according to procedures reported in the literature.[14,15] Analytical and spectroscopic (IR and ^{1}H NMR) data obtained for all six compounds were in agreement with published results. The ^{1}H NMR data showed that **3** was obtained as an ~1:1 mixture of the cis and trans isomers while **4** and **5** were obtained as the pure trans isomers.

X-ray Crystallography. Compounds **1**, **3**, *trans*-**5**, and **6** were dissolved in minimum volumes of acetonitrile, and the solutions were left to stand for 2–3 days. After complete evaporation of the solvent, small crystals suitable for X-ray analysis were formed. In the case of **3**, only crystals of the cis isomer (*cis*-**3**) were obtained. Data collections were performed using an Oxford Diffraction Xcalibur 3 diffractometer equipped with a CCD area detector and Mo Kα radiation (λ = 0.7107 Å), and the program used for this purpose was CrysAlis CCD.[16] For each of the crystals, different runs were conducted in order to collect a complete sphere of data. Data were reduced using the program CrysAlis RED,[17] and the absorption correction was applied with the program ABSPACK.[17] The structures were solved using the Patterson method of SHELXS86,[18] and then the program SHELX97[19] was employed for structure refinement by full-matrix least-squares against F^2 using all of the data.

In **6**, the atoms Au(1), O(1), P(1), F(3), and F(4) lie on special positions, and their population factors were set to 0.5. For **1**, the atoms of the aromatic moiety were fixed to a regular hexagon, while for *cis*-**3**, the carbon atoms were set isotropically because of the otherwise poor ratio of calculated to observed parameters. In all of the other cases, the non-hydrogen atoms were refined anisotropically. The hydrogen atoms in all of the structures were set in calculated positions and refined isotropically.

Geometrical calculations were performed using PARST97,[20] and molecular plots were produced using the program ORTEP3.[21] Crystallographic data and refinement parameters are reported in Table 1.

Solution Studies. UV–vis absorption spectra of the gold(III) compounds were recorded on a Perkin-Elmer Lambda 20 Bio spectrophotometer. Hydrolysis experiments were conducted by adding small amounts of freshly prepared, concentrated solutions

(14) Cinellu, M. A.; Minghetti, G.; Pinna, M. V.; Stoccoro, S.; Zucca, A.; Manassero, M.; Sansoni, M. *J. Chem. Soc., Dalton Trans.* **1998**, 1735.
(15) Cinellu, M. A.; Minghetti, G.; Pinna, M. V.; Stoccoro, S.; Zucca, A.; Manassero, M. *J. Chem. Soc., Dalton Trans.* **2000**, 1261.
(16) *CrysAlis CCD*, version 1.171.29.2; Oxford Diffraction Ltd.: Abingdon, U.K., 2006.
(17) *CrysAlis RED*, version 1.171.29.2; Oxford Diffraction Ltd.: Abingdon, U.K., 2006.
(18) SHELXS-86: Sheldrick, G. M. *Acta Crystallogr.* **1990**, *A46*, 467.
(19) Sheldrick, G. M. *SHELX 97*; University of Göttingen: Göttingen, Germany, 1997.
(20) Nardelli, M. *J. Appl. Crystallogr.* **1995**, *28*, 659.
(21) Farrugia, L. J. *J. Appl. Crystallogr.* **1997**, *30*, 565.

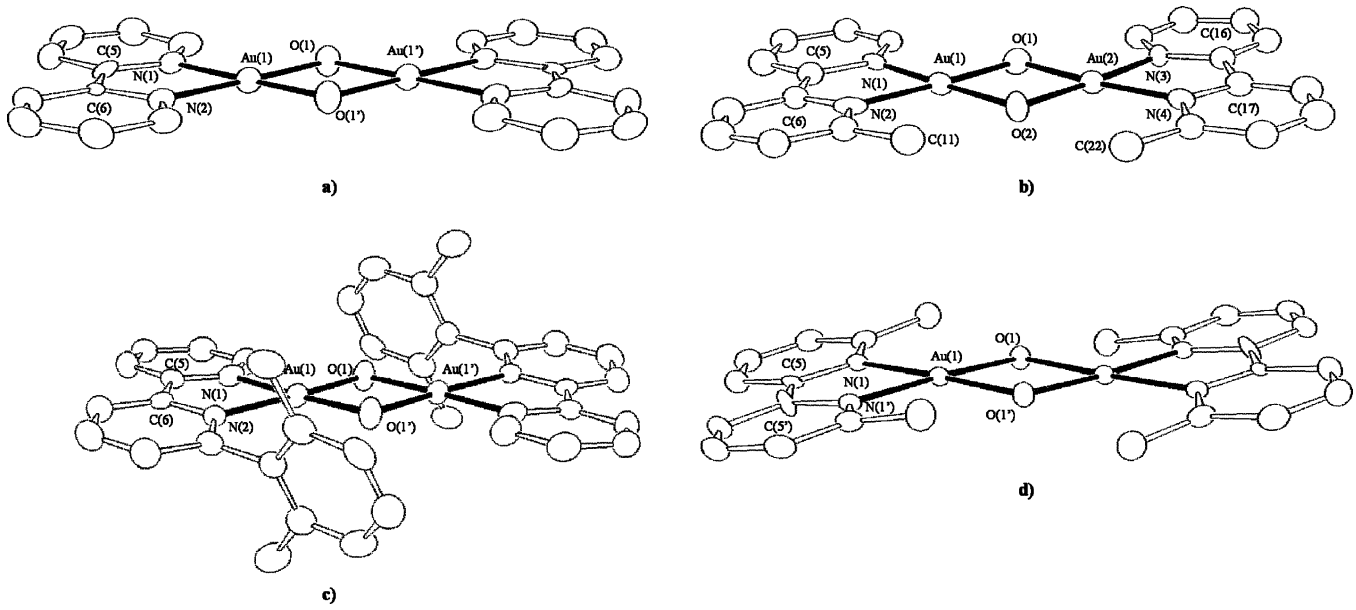

Figure 1. ORTEP drawing (using 30% probability ellipsoids) of the binuclear gold(III) oxo complex cations in (a) **1**, (b) *cis*-**3**, (c) *trans*-**5**, and (d) **6**.

of **1**−**6** in dimethyl sulfoxide (DMSO) to the reference buffer (10 mM phosphate, pH 7.4). Electronic spectra of the resulting mixtures were monitored at 70 °C over 24 h.

Electrochemistry. The apparatus employed for electrochemistry studies has been described elsewhere.[22] Anhydrous 99.9% DMSO was obtained from Aldrich. Electrochemical grade $[NEt_4][PF_6]$ (Fluka) was used as a supporting electrolyte (0.2 M). All potential values are quoted with respect to the saturated calomel electrode (SCE). Under our experimental conditions, the one-electron oxidation of ferrocene occurred at $E^{\circ\prime} = 0.40$ V.

DFT Calculations. Quantum-chemical DFT calculations were performed on bipy; the 4-, 4′-, 6-, and/or 6′-substituted bipy derivatives 6-Mebipy, 6,6′-Me_2bipy, 4,4′-Me_2bipy, and 4,4′,6,6′-Me_4bipy; the $Au_2O_2^{2+}$ fragment; and compounds **1**, *cis*-**3**, *trans*-**3**, and **6**, using the well-known three-parameter B3LYP[23] and mPW1PW[24] hybrid functionals implemented in the commercially available Gaussian03 program suite.[25] Although the use of all-electron basis sets (BSs) provides better accuracy, pseudopotential techniques are useful when relativistic effects must be taken into account. Thus, the double-ζ plus polarization all-electron (pVDZ) BSs of Schäfer, Horn, and Ahlrichs[26] were used for C, H, and N, while the LanL2DZ[27] and CRENBL[28] BSs with relativistic effective core potentials (RECPs) were adopted for the heavier Au species.[29] Geometry optimization was performed when available from structural data. For all of the compounds, NBO populations[30] and Wiberg bond indices[31] were calculated at the optimized geometries.[32] The programs Gabedit 2.0.7[33] and Molden 4.6[34] were used to investigate charge distributions and molecular orbital (MO) shapes.

Results and Discussion

Structural Data. The solid-state structures of **1**, *cis*-**3**, *trans*-**5**, and **6** have been solved here by single-crystal X-ray diffraction analysis, while the structure of *trans*-**4** had been reported in a previous study.[14] Unfortunately, repeated attempts to obtain good quality single crystals for $[Au_2(\mu\text{-}O)_2(4,4'\text{-}tBubipy)_2](PF_6)_2$ (**2**) failed, thus preventing the

(22) Stulz, E.; Saders, J. K. M.; Montalti, M.; Prodi, L.; Zaccheroni, N.; de Biani, F. F.; Grigiotti, E.; Zanello, P. *Inorg. Chem.* **2002**, *41*, 5269.
(23) (a) Becke, A. D. *J. Chem. Phys.* **1993**, *98*, 5648. (b) Lee, C.; Yang, W.; Parr, R. G. *Phys. Rev. B* **1988**, *37*, 785. (c) Vosko, S. H.; Wilk, L.; Nusair, M. *Can. J. Phys.* **1980**, *58*, 1200. (d) Stephens, P. J.; Devlin, F. J.; Chabalowski, C. F.; Frisch, M. J. *J. Phys. Chem.* **1994**, *98*, 11623.
(24) Adamo, C.; Barone, V. *J. Chem. Phys.* **1998**, *108*, 664.
(25) Frisch, M. J.; Trucks, G. W.; Schlegel, H. B.; Scuseria, G. E.; Robb, M. A.; Cheeseman, J. R.; Montgomery, J. A., Jr.; Vreven, T.; Kudin, K. N.; Burant, J. C.; Millam, J. M.; Iyengar, S. S.; Tomasi, J.; Barone, V.; Mennucci, B.; Cossi, M.; Scalmani, G.; Rega, N.; Petersson, G. A.; Nakatsuji, H.; Hada, M.; Ehara, M.; Toyota, K.; Fukuda, R.; Hasegawa, J.; Ishida, M.; Nakajima, T.; Honda, Y.; Kitao, O.; Nakai, H.; Klene, M.; Li, X.; Knox, J. E.; Hratchian, H. P.; Cross, J. B.; Bakken, V.; Adamo, C.; Jaramillo, J.; Gomperts, R.; Stratmann, R. E.; Yazyev, O.; Austin, A. J.; Cammi, R.; Pomelli, C.; Ochterski, J. W.; Ayala, P. Y.; Morokuma, K.; Voth, G. A.; Salvador, P.; Dannenberg, J. J.; Zakrzewski, V. G.; Dapprich, S.; Daniels, A. D.; Strain, M. C.; Farkas, O.; Malick, D. K.; Rabuck, A. D.; Raghavachari, K.; Foresman, J. B.; Ortiz, J. V.; Cui, Q.; Baboul, A. G.; Clifford, S.; Cioslowski, J.; Stefanov, B. B.; Liu, G.; Liashenko, A.; Piskorz, P.; Komaromi, I.; Martin, R. L.; Fox, D. J.; Keith, T.; Al-Laham, M. A.; Peng, C. Y.; Nanayakkara, A.; Challacombe, M.; Gill, W. P. M.; Johnson, B.; Chen, W.; Wong, M. W.; Gonzalez, C.; Pople, J. A. *Gaussian 03*; Gaussian, Inc.: Wallingford, CT, 2004.
(26) Schäfer, A.; Horn, H.; Ahlrichs, R. *J. Chem. Phys.* **1992**, *97*, 2571.
(27) (a) Dunning, T. H., Jr.; Hay, P. J. In *Methods of Electronic Structure Theory*; Schaefer, H. F., III, Ed.; Plenum Press: New York, 1977; Vol. 2. (b) Ortiz, J. V.; Hay, P. J.; Martin, R. L. *J. Am. Chem. Soc.* **1992**, *114*, 2736.
(28) Ross, R. B.; Powers, J. M.; Atashroo, T.; Ermler, W. C.; LaJohn, L. A.; Christiansen, P. A. *J. Chem. Phys.* **1990**, *93*, 6654.
(29) Basis sets were obtained from the Extensible Computational Chemistry Environment Basis Set Database, version 02/02/06, as developed and distributed by the Molecular Science Computing Facility of the William R. Wiley Environmental and Molecular Sciences Laboratory, which is a part of the Pacific Northwest National Laboratory, P.O. Box 999, Richland, WA 99352, and funded by the U.S. Department of Energy. The Pacific Northwest National Laboratory is a multiprogram laboratory operated by Battelle Memorial Institute for the U.S. Department of Energy under Contract DE-AC06-76RLO 1830. Contact Karen Schuchardt for further information.
(30) (a) Reed, A. E.; Weinhold, F. *J. Chem. Phys.* **1983**, *78*, 4066. (b) Reed, A. E.; Weinstock, R. B.; Weinhold, F. *J. Chem. Phys.* **1985**, *83*, 735. (c) Reed, A. E.; Curtiss, L. A.; Weinhold, F. *Chem. Rev.* **1988**, *88*, 899.
(31) Wiberg, K. *Tetrahedron* **1968**, *24*, 1083.
(32) Glendening, E. D.; Reed, A. E.; Carpenter, J. E.; Weinhold, F. *NBO*, version 3.1.
(33) Allouche, A.-R. *Gabedit*, a free graphical user interface for computational chemistry packages (available from http://lasim.univ-lyon1.fr/allouche/gabeditb).
(34) Schaftenaar, G.; Noordik, J. H. *J. Comput.-Aided Mol. Des.* **2000**, *14*, 123.

Table 2. Selected Bond Lengths (Å) and Angles (deg) for Compounds **1**, *cis*-**3**, *trans*-**4**, *trans*-**5**, and **6**

length/angle	**1**[a]	*cis*-**3**[b]	*trans*-**4**[c,d]	*trans*-**5**	**6**
Au(1)−Au(2)[Au(1′)]	2.9573(6)	3.0165(7)	3.017(1)	2.9963(6)	3.044(1)
O(1)−O(2)[O(1′)]	2.585(8)	2.51(1)	2.529	2.558(8)	2.45(1)
Au(1)−O(1)	1.971(5)	1.972(7)	1.976(3)	1.962(6)	1.955(5)
Au(1)−O(2)[O(1′)]	1.957(6)	1.976(7)	1.961(3)	1.977(6)	
Au(1)−N(1)	2.015(4)	1.99(1)	2.011(4)	2.023(7)	2.065(6)
Au(1)−N(2)[N(1′)]	2.000(4)	2.071(9)	2.100(3)	2.081(7)	
Au(2)−O(1)		1.931(7)			
Au(2)−O(2)		1.975(7)			
Au(2)−N(3)		2.017(9)			
Au(2)−N(4)		2.028(9)			
Au(1)−O(1)−Au(2)[Au(1′)]	97.7(2)	101.2(3)	100.0(1)	99.0(2)	102.3(3)
O(1)−Au(1)−N(1)	98.1(2)	95.4(3)	94.2(1)	94.7(3)	100.8(3)
O(1)−Au(1)−N(2)	178.9(2)	175.8(3)	174.0(1)	174.3(2)	
O(1)−Au(1)−O(2)[O(1′)]	82.3(2)	79.1(3)	80.0(1)	81.0(2)	77.7(3)
N(1)−Au(1)−N(2)[N(1″)]	80.8(2)	80.4(4)	80.3(1)	79.6(3)	80.4(4)
N(1)−Au(1)−O(2)[O(1′)]	179.2(2)	174.2(3)	174.1(1)	175.6(2)	176.3(2)
N(2)−Au(1)−O(2)[O(1′)]	98.8(2)	105.1(3)	105.5(1)	104.8(2)	
O(1)−Au(2)−N(3)		95.2(3)			
O(1)−Au(2)−N(4)		174.5(3)			
O(1)−Au(2)−O(2)		80.1(3)			
N(3)−Au(2)−N(4)		79.6(4)			
N(3)−Au(2)−O(2)		175.3(3)			
N(4)−Au(2)−O(2)		105.0(3)			

[a] For **1**, ′ = $-x$, $-y + 1$, $-z$. [b] For **3**, ′ = $-x$, $-y$, $-z + 1$. [c] Data from ref 14. [d] For **4**, ′ = $-x$, $-y$, $-z$ and ″ = x, $-y$, z.

determination of its crystal structure. ORTEP views of the binuclear gold(III) oxo complex cations in **1**, *cis*-**3**, *trans*-**5**, and **6** are shown in Figure 1.

The asymmetric units (a.u.'s) of **1** and *trans*-**5** contain half of the metallic complex, one hexafluorophosphate anion, and one acetonitrile molecule. The entire metal complex, two hexafluorophosphate anions, and one acetonitrile molecule are present in the a.u. of *cis*-**3**. One-fourth of the metal complex and half of a hexafluorophosphate anion have been identified in the a.u. of **6**.

A common structural feature for all of these binuclear gold(III) complexes is the presence of an extended, roughly planar system containing the Au_2O_2 "diamond core" and the aromatic rings of the bipyridine ligands. This structural motif is well-conserved throughout all of the investigated compounds.

Here we compare the structural parameters of *cis*-**3**, *trans*-**5**, and **6** as well as those reported previously for *trans*-**4**[14] to those of the parent complex **1**, which is considered to be the reference compound. Selected bond distances and angles are compiled in Table 2 in order to highlight the effects of the various substituents on the structural parameters.

Because of the presence of an inversion center in **1**, **5**, and **6**, the Au_2O_2 ring turns out to be planar.[35] For complex **3**, the deviation of the Au_2O_2 moiety from planarity is not significant. An interesting feature of this structural moiety is the relationship between the Au···Au and O···O distances across the series of compounds. In fact, as the distance between the two metal atoms progressively increases in the order **1** < *trans*-**5** < *cis*-**3** < *trans*-**4** < **6** (see Table 2), the value of the corresponding O···O distance decreases accordingly.

The coordination at both gold(III) centers is essentially square planar; the largest deviation from the best plane containing the coordination ion is found for Au(1) in *trans*-**5**, where the gold ion is 0.14 Å out of the plane. The five-membered Au(1)−N(1)−C(5)−C(6)[C(5′)]−N(2)[N(1′)] ring in each of the complexes [as well as the pairwise Au(2)−N(3)−C(16)−C(17)−N(4) ring in *cis*-**3**] is also virtually planar [with a maximum deviation of 0.06 Å for C(5) in **6**]. The ring is also coplanar with the Au_2O_2 moiety [with a maximum deviation of 2.5(2)° for *cis*-**3**] except in the case of **6**, where the two planes form an angle of 6.44(9)°. In *trans*-**5**, the xylyl ring is nearly perpendicular [76.1(2)°] to the bipyridine moiety.

The Au···Au distances, which range from 2.96 to 3.04 Å, are much shorter than the sum of the estimated van der Waals radii for two gold atoms (3.60 Å) and also shorter than those found in a variety of binuclear complexes containing a planar $Au_2(XR_n)_2$ (XR_n = NR_2, OR, SR, Cl, Br) unit,[35,36] thus indicating a weak Au···Au interaction.

The two Au−N bond lengths in **1** are quite similar: 2.01 and 2.00 Å for Au(1)−N(1) and Au(1)−N(2), respectively. In *cis*-**3**, *trans*-**5**, and **6**, introduction of alkyl or aryl substituents at the 6 position of 2,2′-bipyridine causes a significant increase in the Au−N distance adjacent to the substituent (e.g., to 2.07 Å in **6**), while the other Au−N distance in both *cis*-**3** and *trans*-**5** remains almost unchanged from that of **1**; the same trend was found in **4**. In contrast, a very small difference in the two Au−O bond lengths is seen in all of the complexes except **3**; the average value (1.97 Å) is the same found in some gold(III) alkoxo complexes

(35) For an exhaustive discussion of the bending angle between the coordination planes of the two metal atoms in binuclear square planar complexes of d^8 transition-metal ions with unsubstituted bridges, see: Aullón, G.; Ujaque, G.; Lledós, A.; Alvarez, S.; Alemany, P. *Inorg. Chem.* **1998**, *37*, 804.

(36) A search of the Cambridge Structural Database [CSD version 5.28 (Allen, F. H. *Acta Crystallogr.* **2002**, *B58*, 380)] retrieved 11 hits, of which only three had an OR bridge. One of these was *trans*-**4** (R = none); the others were hydroxo-bridged complexes featuring Au···Au distances in the range 3.15–3.43 Å.

supported by 2,2′-bipyridines.[14,15,37] In **3**, one of the four Au−O distances [O(1)−Au(2)] is considerably shorter (1.93 Å), while the other three are almost identical to each other. Another effect of the presence of a substituent on the bipyridine ligand is an increase in the N−Au−O angle facing the substituent itself. In **1**, the N(1)−Au(1)−O(1) and N(2)−Au(1)−O(2) angles are 98.1(2) and 98.8(2)°, respectively, while in **6**, they are both 102.3(3)°. The N(2)−Au(1)−O(2)[O(1′)] angle in *cis*-**3** and *trans*-**5** [and the N(4)−Au(2)−O(2) angle in *cis*-**3**] is wider than the N(1)−Au(1)−O(1) [and *cis*-**3** N(3)−Au(2)−O(1)] angle (∼105 vs ∼95°). These differences (increases in the Au−N bond distance and the N−Au−O angle) might be ascribed to the need to minimize steric hindrance caused by the substituent. This explanation is also suggested by the short intramolecular contacts found in *cis*-**3** and **6** involving the methyl pendant arms. In *cis*-**3**, O(2) is 2.88 Å from C(11) and 2.84 Å from C(22), while in **6**, the C(6)···O(1) contact is 2.81 Å; these distances indicate a weak hydrogen-bonding interaction.[38]

Finally, various types of intramolecular and intermolecular interactions were detected in the lattices of *cis*-**3** and *trans*-**5**. Stacking interactions (both "offset π-stacked"-type[39] and CH/π interactions[40]) between symmetry-related molecules were identified in the crystal lattices of the complexes. An example of this latter kind of interaction in *cis*-**3** is provided by the distance between hydrogen atom H(11a) and Ct1 (where Ct1 is the geometric centroid for an aromatic ring in the molecule reported by $-x + 1, -y, -z$), which is 2.84 Å. On the other hand, the distance between the centroids Ct2 and Ct3 for the stacked aromatic rings is 4.03 Å. Moreover, in *cis*-**3**, an intermolecular interaction of 3.45 Å is found between Au(2) and O(2′) of a symmetry-related molecule (reported by $-x + 1, -y, -z$). (These interactions in *cis*-**3** are illustrated in Figure S1 in the Supporting Information.) In *trans*-**5**, the CH/π interaction involves hydrogen atom H(1) of the bipyridine ligand and the aromatic xylyl ring of the same molecule, for which the H(1)···Ct1 distance is 2.99 Å. The stacking interaction involves xylyl rings of the original molecule and the molecule reported by $-x, -y, -z$; in this case, the distance between the centroids Ct1 and Ct2 is 4.06 Å. (Figure S2 in the Supporting Information illustrates the interactions in *trans*-**5**.)

Solution Studies: Comparative Analysis of Thermal Stability Profiles. Some relevant aspects of the solution behavior of these binuclear gold(III) compounds were described in our previous study.[13] In particular, time-dependent spectrophotometric analyses of their ligand-to-metal charge transfer transitions in the 300–350 nm region clearly showed that these compounds are essentially stable for at least 24 h in 10 mM phosphate buffer (pH 7.4) at 37 °C.[13]

In the present work, we have extended those studies by analyzing the comparative stabilities of all of these compounds in aqueous solution at physiological pH using a temperature of 70 °C. Notably, at this temperature, the overall stabilities of the various species are strongly decreased, enabling a quick comparative assessment of their propensities/resistances toward reductive decomposition to metallic gold. In all cases, a progressive decrease in the intensity of the main transition at 300–350 nm along with a concomitant increase in the intensity of the broad band around 550 nm due to buildup of metallic gold produced by reduction of gold(III) was observed. Representative time-dependent spectral profiles for these degradation processes are shown in Figure 2.

It is quite evident that the six investigated binuclear gold(III) complexes manifested substantially different kinetic stabilities with respect to thermally induced degradation/reduction processes. The differential stability of these complexes, monitored over 24 h, is best described by the half-lives for the disappearance of the main absorption band at 70 °C (Figure 2 inset). It is noteworthy that **2** and **6** were the most- and least-stable complexes, respectively.

Electrochemical Properties. The electrochemical behavior of the present oxo-bridged binuclear gold(III) compounds was investigated in detail in comparison with that of the mononuclear precursor of **1**,[15] [Au(bipy)(OH)$_2$][PF$_6$] (**OH1**). As shown in Figure 3, this species exhibited two main reduction processes in DMSO solution. One of these, an irreversible reduction at −0.60 V, was assigned as Au(III)-centered; the other reduction, which manifested partial chemical reversibility, was attributed to the bipyridine ligand, in agreement with previous findings.[41,42] The minor peak labeled with an asterisk in Figure 3 was ascribed to an adsorption process, as indicated by its linear increase with the scan rate.[43]

Exhaustive reduction around the irreversible cathodic step ($E_w = -0.7$ V) consumed 1.7 electrons per molecule. As a consequence, the original pale-yellow solution turned a pale pink color. Concomitantly, a brown-yellow solid typical of Au(0) deposition was deposited on the macroelectrode surface. In agreement with the evident irreversibility of this process, cyclic voltammograms recorded on the resulting solution showed the appearance of a new reversible reduction ($E^{\circ\prime} = -1.2$ V) that could not be assigned to the free bipyridine ligand (see the redox potentials for the free bipyridine ligands in Table 3). It must be pointed out that in nonaqueous solvents, the reduction of Au(III) complexes usually proceeds through two distinct steps, Au(III) → Au(I) and Au(I) → Au(0),[44–46] as seen for **OH1** in acetonitrile solution.[42] In the present case, the reversible reduction that appeared after exhaustive electrolysis

(37) Cinellu, M. A.; Minghetti, G.; Cocco, F.; Stoccoro, S.; Zucca, A.; Manassero, M. *Angew. Chem., Int. Ed.* **2005**, *44*, 6892.
(38) Desiraju, G. R.; Steiner, T. *The Weak Hydrogen Bond*; Oxford University Press: Oxford, U.K., 1999.
(39) Janiak, C. *J. Chem. Soc., Dalton Trans.* **2000**, 3885–3896.
(40) Takahashi, O.; Kohno, Y.; Iwasaki, S.; Iwaoka, M.; Tomoda, S.; Umezawa, Y.; Tsuboyama, S.; Nishio, M. *Bull. Chem. Soc. Jpn.* **2001**, *74*, 2421.
(41) Sanna, G.; Pilo, M. I.; Spano, N.; Minghetti, G.; Cinellu, M. A.; Zucca, A.; Seeber, R. *J. Organomet. Chem.* **2001**, *622*, 47.
(42) Sanna, G.; Pilo, M. I.; Minghetti, G.; Cinellu, M. A.; Spano, N.; Seeber, R. *Inorg. Chim. Acta* **2000**, *310*, 34.
(43) Zanello, P. *Inorganic Electrochemistry: Theory, Practice and Application*; RSC: Oxford, U.K., 2003; p 615.
(44) Koelle, U.; Laguna, A. *Inorg. Chim. Acta* **1999**, *290*, 44.
(45) Ronconi, L.; Marzano, C.; Zanello, P.; Corsini, M.; Miolo, G.; Maccà, C.; Trevisan, A.; Fregona, D. *J. Med. Chem.* **2006**, *49*, 1648.
(46) Bortoluzzi, M.; De Faveri, E.; Daniele, S.; Pitteri, B. *Eur. J. Inorg. Chem.* **2006**, 3393.

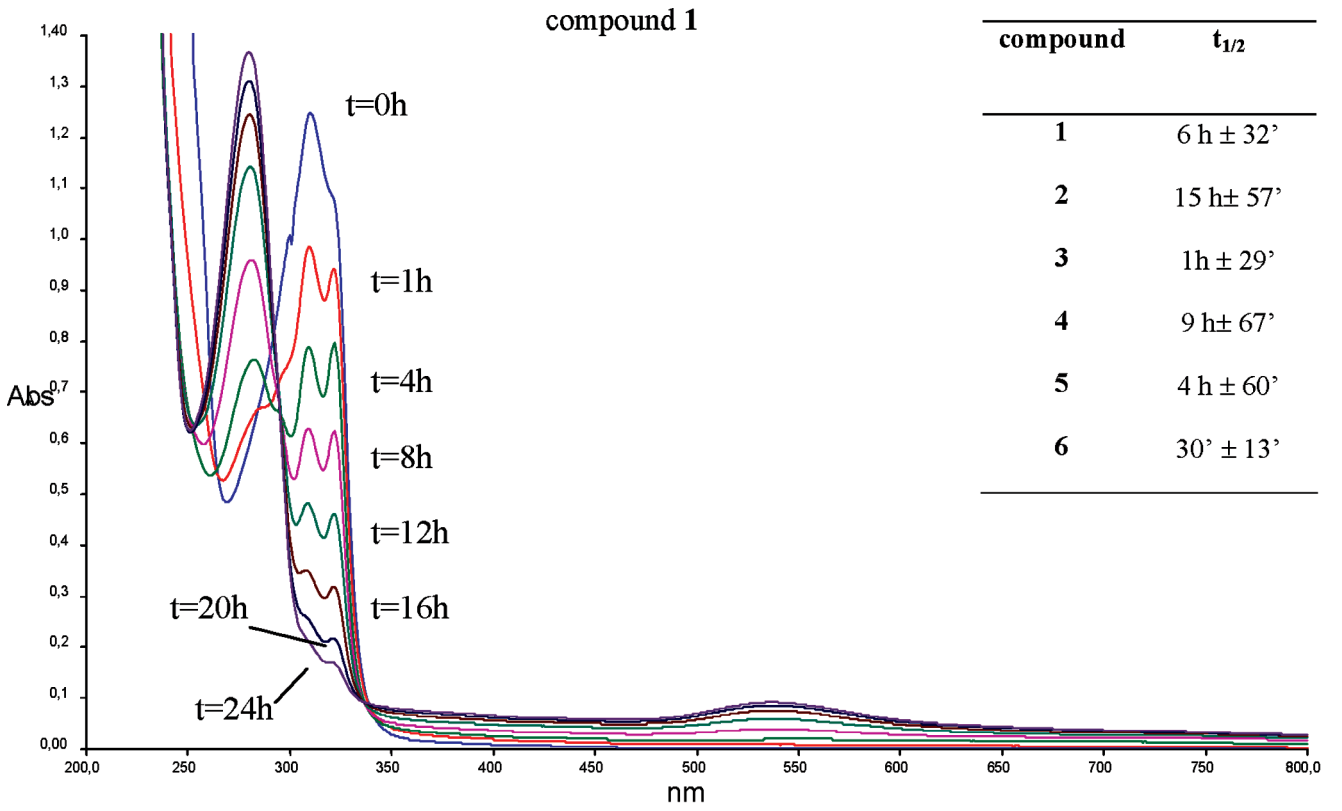

compound	$t_{1/2}$
1	6 h ± 32’
2	15 h± 57’
3	1h ± 29’
4	9 h± 67’
5	4 h ± 60’
6	30’ ± 13’

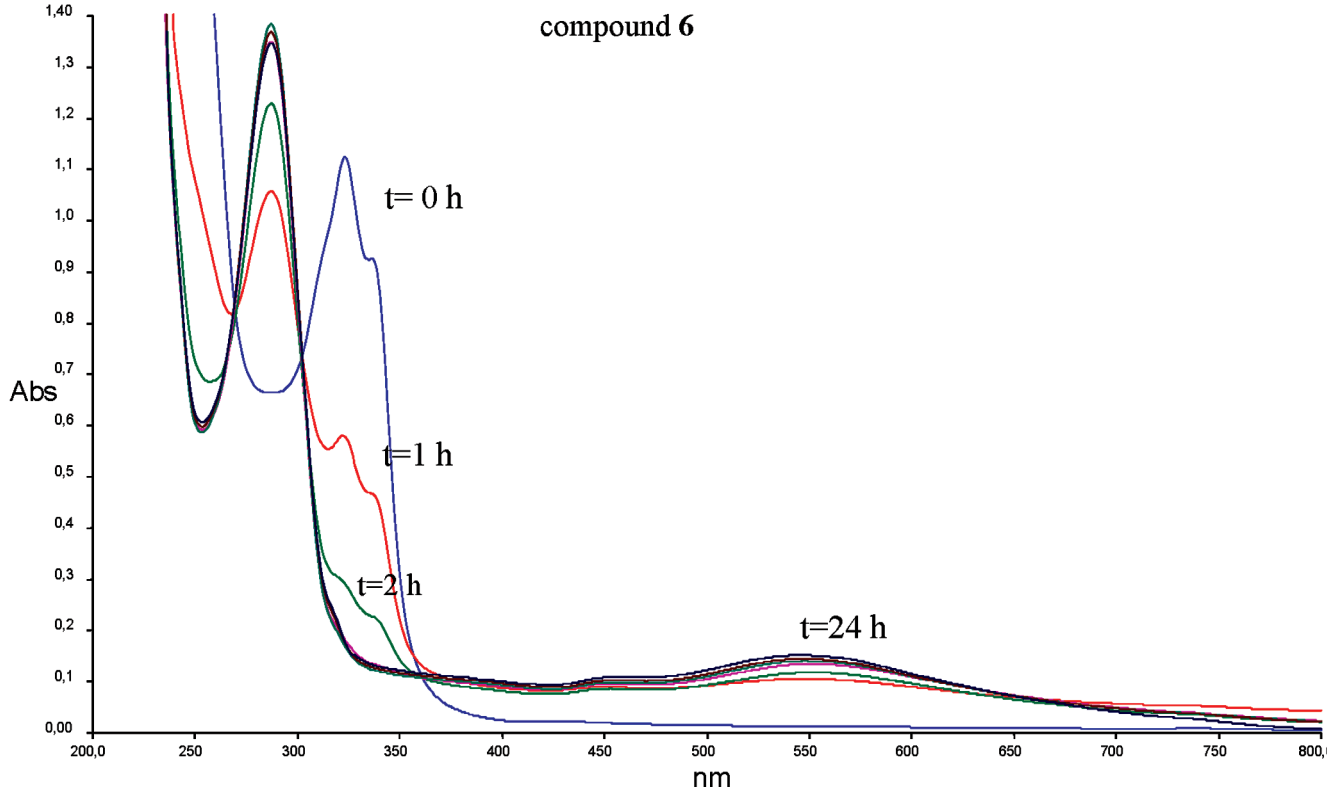

Figure 2. Representative hydrolysis profiles of **1** and **6** (initial concentration 5×10^{-5} M in 10 mM phosphate buffer, pH 7.4) at 70 °C. Spectra were recorded at various times over a period of 24 h. The inset shows estimated half-lives ($t_{1/2}$) for compounds **1**−**6**. Data are reported as average ± SD of three separate experiments.

was assigned to a reorganized Au(III) complex having a 1:2 Au:bipy composition. It is worth noting that in a few cases, the direct Au(III) → Au(0) process has also been observed.[41,42]

As exemplified by the cyclic voltammetric response for **1** shown in Figure 4, all of the binuclear species exhibited two irreversible reduction processes. Notably, the second reduc-

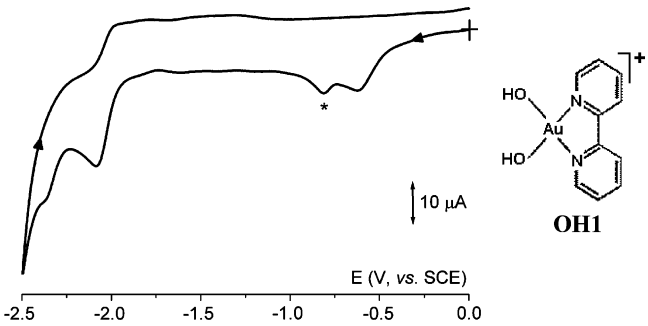

Figure 3. Cyclic voltammogram recorded at a platinum electrode in a 1×10^{-3} M solution of **OH1** in DMSO, with $[NEt_4][PF_6]$ (0.1 M) as a supporting electrolyte. The scan rate was 0.2 V/s.

Table 3. Peak Potential Values (V vs SCE) for Reduction Processes Exhibited by the Present Au(III) Complexes in DMSO Solution and Their Free Bipyridine Ligands

compound	E_{pc} for first irreversible reduction	E_{pc} for second irreversible reduction	$E^{\circ\prime}$ for reversible reduction	$E^{\circ\prime}$ for free bipyridine ligand
OH1	−0.60	−	−2.02	−2.06
1	−0.44	−0.76	−	−2.06
2	−0.53	−0.82	−	−2.14
3	−0.41	−0.71	−2.11	−
4	−0.40	−0.69	−2.12	−
5	−0.51	−0.65	−2.04	−
6	−0.27	−0.6[a]	−2.12	−2.13

[a] Measured at 2.0 V/s.

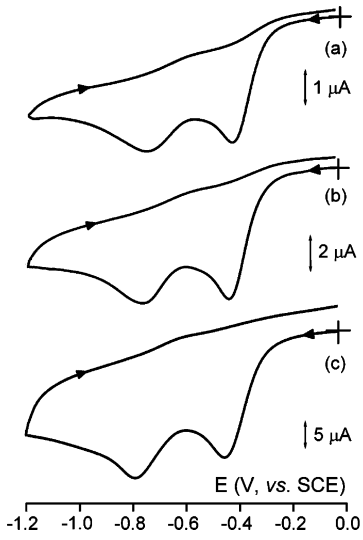

Figure 4. Cyclic voltammograms recorded at a platinum electrode in a 9×10^{-4} M solution of **1** in DMSO, with $[NEt_4][PF_6]$ (0.1 M) as a supporting electrolyte, at scan rates of (a) 0.05, (b) 0.2, and (c) 2.0 V/s.

tion tended to increase progressively with increasing scan rate, reaching a peak ratio of ∼1 with respect to the first reduction, at scan rates depending on the nature of the binuclear complex. For instance, as shown in Figure 4, the peak-current ratio for the second and first processes increased from 0.4 to 0.5 to 0.7 as the scan rate increased from 0.05 to 0.2 to 2.0 V/s. Ratio values near 1 were reached only at scan rates higher than 5 V/s. This means that the species that was electrogenerated in the first reduction step tends to decompose; this chemical complication was largely prevented only at high scan rates.

All attempts to determine the number of electrons involved in the first reduction process using controlled potential coulometry failed because of absorption effects. In fact, exhaustive electrolysis consumed ∼0.9–1.5 electrons per molecule, depending on the nature of the complex, and was accompanied by electrodeposition of a dark-brown material. Such a drawback is rather common in electrochemical studies of Au(III) complexes.

For **1** and **2**, no bipyridine-centered reductions were detected (as Figure 4 demonstrates in the case of **1**). As shown in Table 3, the binuclear complexes in **3**−**6** displayed one additional reduction process that was reliably centered on the bipyridine ligand. Electrode potentials for all of the pertinent reduction processes are compiled in Table 3.

Within the necessarily limited interpretation of the possible redox processes that may take place for the binuclear complexes, the appearance of two Au(III)-centered reductions suggests that the two gold centers are not electronically independent.[47] It seems plausible that they could mutually exchange electrons across the oxygen bridges or by a Au···Au interaction through space. Attempts to correlate electrochemical and crystallographic data failed to resolve whether the interaction occurred through bonds or through space. Actually, under the assumption of a thermodynamic meaning of the peak potential values, diagrams showing the electrode potentials for the first reduction as functions of the Au−O−Au angles, the Au···Au distances, and the O···O distances did not afford univocal, linear correlations (the measured correlation coefficients were 0.78, 0.70, and 0.87, respectively).

As expected, the nature and position of the substituents present on the bipyridine ligands play an active role in determining the electrode potentials. In particular, we note that **6** undergoes reduction at a sufficiently low potential value ($E_p = -0.27$ V vs SCE in DMSO would correspond to $E_p = -0.25$ V vs NHE in aqueous solution) to make its spontaneous reduction inside cells feasible (the reducing ability of the cellular environment is evaluated at $E^\circ = -0.24$ V vs NHE).[48] This implies that the anticancer activity of this compound could also be triggered through the mechanism commonly known as "activation by reduction".[49]

The electrochemical results reported above prompted us to check whether these gold(III) oxo complexes could actually be reduced by glutathione and citric acid, two reducing agents that are present in cells at relatively intracellular high concentrations. Spectrophotometric experiments were limited to compounds **1** and **6** in the presence of a 10-fold molar excess of each reducing agent. We observed that both complexes were quickly and completely reduced by glutathione (the process was nearly complete after

(47) It may be suggested that reduction of the first Au(III) center might trigger the release of the second Au(III) fragment. In our judgment, it is plausible that this process may occur on time scales longer than that of cyclic voltammetry, but we have ruled out the possibility that the second reduction is centered on the released Au(III) fragment on the basis of the fact that the height of the second reduction peak progressively increases with increasing scan rate.

(48) Shafer, F. Q.; Buettner, G. R. *Free Radical Biol. Med.* **2001**, *30*, 119.
(49) (a) Clarke, M. J. *Met. Ions Biol. Syst.* **1980**, *11*, 231. (b) Mestroni, G.; Alessio, E.; Sava, G.; Pacor, S.; Coluccia, M. In *Metal Complexes in Cancer Chemotherapy*; Keppler, B. K., Ed.; VCH: Weinheim, Germany, 1993; pp 157–185. (c) Galanski, M. *Anti-Cancer Agents Med. Chem.* **2007**, *7*, 1.

Table 4. NBO Charges (e) on the Donor Nitrogen Atoms and Eigenvalues (hartree) of HOMOs and HOMO-1's Calculated for bipy, 6-Mebipy, 6,6′-Me_2bipy, 4,4′-Me_2bipy, and 4,4′,6,6′-Me_4bipy (See Chart 1) Using DFT[a]

molecule	Q_N	$Q_{N'}$	ϵ_{HOMO-1}[b]	ϵ_{HOMO}[b]
bipy	−0.453	−0.453	−0.2440	−0.2406
6-Mebipy	−0.470	−0.455	−0.2391	−0.2379
6,6′-Me_2bipy	−0.471	−0.471	−0.2356	−0.2350
4,4′-Me_2bipy	−0.459	−0.459	−0.2388	−0.2356
4,4′,6,6′-Me_4bipy	−0.477	−0.477	−0.2309	−0.2303

[a] DFT calculations used the B3LYP functional with Schäfer−Horn−Ahlrichs pVDZ BSs for C, H, and N. [b] In the C_{2v} point group, the HOMO and the HOMO-1 belong to the b_2 and a_2 representations, respectively, for all of the molecules except 6,6′-Me_2bipy and 4,4′,6,6′-Me_4bipy, for which the representations of the two MOs are switched.

10 min). In contrast, after 24 h of reaction with citric acid, almost all of **6** but only ∼50% of **1** was reduced. Interestingly, the rate of the reduction process with citric acid was far slower, with a half-life of ∼4 h for **6**.

Theoretical Studies. In recent years, it has been shown that DFT calculations can be successfully exploited to evaluate the donor ability of different polypyridyl substrates toward Lewis acids ranging from unsaturated metal complexes to halogens and interhalogens.[50] In particular, key aspects are the composition of the highest occupied molecular orbitals (HOMOs) and the molecular charge distribution, which can be usefully evaluated on the basis of natural bond orbital analysis.[25] In order to gain insight into the effect of introducing alkyl substituents on the reactivity of 2,2′-bipyridine, we have performed DFT calculations on the 2,2′-bipyridine substrates bipy, 6-Mebipy, 6,6′-Me_2bipy, 4,4′-Me_2bipy, and 4,4′,6,6′Me_4bipy, which are variously substituted with methyl groups at the 4, 4′, 6, and 6′ positions (Chart 1).

In 2,2′-bipyridine (considered to have C_{2v} symmetry), the b_2 HOMO is σ in nature and located on both nitrogen atoms, which carry a substantial negative charge. The results summarized in Table 4 reveal that sequential introduction of one or two methyl substituents at the 6 and 6′ positions causes a progressive increase in the eigenvalues of both the b_2 HOMO and the a_2 HOMO-1. Indeed, the energy of the a_2 MO increases by a greater amount than the energy of the b_2 MO, with the result that in 6,6′-Me_2bipy and 4,4′,6,6′-Me_4bipy the energy order of the two orbitals is reversed and the σ-in-nature b_2 MO (depicted for 6,6′-Me_2bipy in Figure 5) is the HOMO-1. Moreover, the introduction of methyl groups at the 6 and 6′ positions causes the nitrogen atom adjacent to the methylated carbon to become more negatively charged, increasing its donor capability. Not surprisingly, the effect of methylation at the 4 and 4′ positions is much less remarkable.

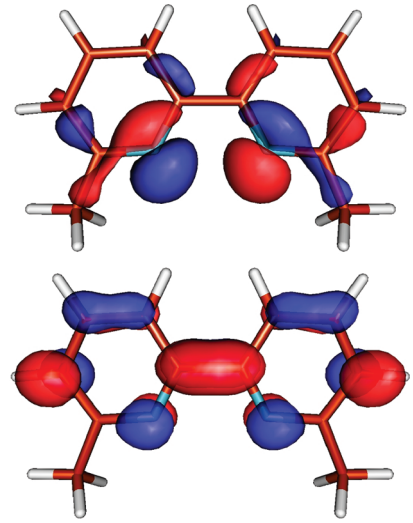

Figure 5. Isosurfaces of the (top) b_2 HOMO-1 and (bottom) b_1 LUMO calculated for 6,6′-Me_2bipy (contour value 0.05 e).

The calculations have been extended to gold(III) oxo complexes. In a recent paper,[51] comparative DFT calculations performed on complexes of the type $[Au(bipy)(C_2H_4)]^+$ using different hybrid functionals and BSs showed that the mPW1PW functional[24] gave the most reliable results when the CRENBL basis set with RECPs[28] was adopted for the metal center. In order to verify whether this approach could be applied to the binuclear gold(III) oxo complexes, the structure of **1** was optimized with both B3LYP[23] and mPW1PW[24] hybrid functionals, adopting LanL2DZ[27] and CRENBL[28] BSs with RECPs for the metal center and Schäfer−Horn−Ahlrichs pVDZ[26] BSs for the remaining atomic species. A comparison of experimental and calculated bond lengths and angles (see Figure S3 and Table S1 in the Supporting Information) showed that all of the optimized distance and angle values were very close to the corresponding experimental ones and that the best results were obtained using the mPW1PW functional and the CRENBL BS for Au, thus confirming the conclusions of the previous work.[51]

On the basis of these results, DFT/mPW1PW calculations were performed on *cis*-**3**, *trans*-**3**, and **6**. Selected optimized bond lengths and angles for the four model complexes, which show very good agreement with the corresponding structural data, are summarized in Table 5.

In agreement with the structural results discussed above, introducing alkyl substituents at the 6 and 6′ positions of 2,2′-bipyridine slightly affected the geometrical parameters calculated for the resulting complexes in comparison with those for **1**. As expected, introduction of a single methyl substituent in the 2,2′-bipyridine ligand caused a slight asymmetry in some of the bond lengths involving the metal center (e.g., Au−N). Nevertheless, it is worth noting that progressive alkylation resulted in only slight increases in the Au···Au distances (e.g., from 3.004 Å in **1** to 3.096 Å in **6**). Indeed, notwithstanding the fact that 6- and 6,6′-methylation increases the donor ability of the resulting substituted 2,2′-bipyridines, the average Au−N distance

(50) (a) Aragoni, M. C.; Arca, M.; Demartin, F.; Devillanova, F. A.; Graiff, C.; Isaia, F.; Lippolis, V.; Tiripicchio, A.; Verani, G. *J. Chem. Soc., Dalton Trans.* **2001**, 2671. (b) Aragoni, M. C.; Arca, M.; Champness, N. R.; De Pasquale, M.; Devillanova, F. A.; Isaia, F.; Lippolis, V.; Oxtoby, N. S.; Wilson, C. *Cryst Eng Comm* **2005**, *7*, 363. (c) Aragoni, M. C.; Arca, M.; Devillanova, F. A.; Hursthouse, M. B.; Huth, S. L.; Isaia, F.; Lippolis, V.; Mancini, A.; Ogilvie, H. R.; Verani, G. *J. Organomet. Chem.* **2005**, *690*, 1923.

(51) Cinellu, M. A.; Minghetti, G.; Cocco, F.; Stoccoro, S.; Zucca, A.; Manassero, M.; Arca, M. *Dalton Trans.* **2006**, 5703.

Table 5. DFT-Optimized[a] Bond Lengths (Å) and Angles (deg) for **1**, *cis*-**3**, *trans*-**3**, and **6**

length/angle[b]	**1**	*cis*-**3**[c]	*trans*-**3**[c]	**6**
Au(1)−Au(2)	3.004	3.044	3.037	3.096
Au(1)−O(1)	1.971	1.967	1.966	1.975
Au(1)−O(2)	1.971	1.981	1.982	1.975
Au(1)−N(1)	2.043	2.034	2.031	2.099
Au(1)−N(2)	2.043	2.093	2.093	2.099
O(1)−O(2)	2.553	2.514	2.522	2.454
Au(1)−O(1)−Au(2)	99.28	101.37	100.58	103.18
Au(1)−O(2)−Au(2)	99.28	100.43	100.58	103.18
O(1)−Au(1)−N(1)	99.73	95.30	95.31	101.64
O(2)−Au(1)−N(2)	99.73	105.65	105.43	101.64
O(1)−Au(1)−N(2)	179.55	175.28	175.15	178.46
O(2)−Au(1)−N(1)	179.55	174.37	174.73	178.46
O(1)−Au(1)−O(2)	80.72	79.07	79.42	76.82
N(1)−Au(1)−N(2)	79.81	79.98	79.84	79.89

[a] DFT calculations used the mPW1PW functional with the CRENBL+RECP BS for Au and Schäfer−Horn−Ahlrichs pVDZ BSs for C, H, N, and O. [b] Atom labeling refers to Figure 1b. [c] The total electronic energies of *cis*-**3** and *trans*-**3** differed by less than 1.5 kcal/mol.

Table 6. NBO Charges (e) for Selected Atoms (Q_j),[a] the Bipyridine Ligands (Q_{bipy}), and the $Au_2O_2^{2+}$ Core ($Q_{Au_2O_2}$) and Energy Eigenvalues (hartree) for the HOMO and LUMO (ϵ_{HOMO} and ϵ_{HOMO}, Respectively) Calculated[b] for **1**, *cis*-**3**, *trans*-**3**, and **6**

	1	*cis*-**3**	*trans*-**3**	**6**
Q_{Au}	1.278	1.278	1.274	1.268
$Q_{O(1)}$	−0.892	−0.880	−0.888	−0.863
$Q_{O(2)}$	−0.892	−0.903	−0.888	−0.863
$Q_{N(1)}$	−0.539	−0.535	−0.533	−0.555
$Q_{N(2)}$	−0.539	−0.555	−0.558	−0.555
Q_{bipy}	0.614	0.613	0.614	0.595
$Q_{Au_2O_2}$	0.772	0.773	0.772	0.810
ϵ_{HOMO}	−0.4648	−0.4672	−0.4669	−0.4654
ϵ_{LUMO}	−0.3041	−0.3020	−0.3003	−0.3103

[a] Atom labeling refers to Figure 1b. [b] DFT calculations used the mPW1PW functional with the CRENBL+RECP BS for Au and Schäfer−Horn−Ahlrichs pVDZ BSs for C, H, N, and O.

underwent a slight but systematic increase with increasing methylation. This increase might be attributable to the concomitant effects of steric hindrance due to the substituents and an increase in the energy difference between the 2,2′-bipyridine filled σ-type donor MO (the HOMO for bipy) and the lowest unoccupied MO (LUMO) of the $Au_2O_2^{2+}$ core having the proper symmetry (the LUMO+1 for $Au_2O_2^{2+}$); at the geometry optimized for **1**, $\epsilon_{HOMO} = -0.236$ hartree for bipy and $\epsilon_{LUMO+1} = -0.644$ hartree for $Au_2O_2^{2+}$. Table 6 reports the NBO charges on the Au, O, and N atoms along with the HOMO and LUMO energy eigenvalues for **1**, *cis*-**3**, *trans*-**3**, and **6**. Selected Wiberg bond indices for these compounds are given in Table S2 in the Supporting Information.

The very modest variation in the Au−N bond lengths is reflected in the constancy of the amount of charge donated from the neutral 2,2′-bipyridine ligands to the $Au_2O_2^{2+}$core, as calculated for **1**, **3**, and **6** (Table 6).[52] As a consequence, the nature of the frontier orbital is also unaffected by 6,6′-alkylation. As an example, the Kohn–Sham (KS) HOMO and LUMO calculated for **6** are depicted in Figure 6. These frontier orbitals can be described as originating from the interaction of the fragment molecular orbitals (FMOs) of the 2,2′-bipyridine ligands and the $Au_2O_2^{2+}$ core. In particular, if the gold oxo complex is considered to belong to the idealized D_{2h} point group, the highest-energy occupied FMO (the FHOMO) of the $Au_2O_2^{2+}$ fragment, which results from the out-of-phase combination of the $2p_z$ atomic orbitals (AOs) of the oxygen atoms with the $5d_{yz}$ AOs of the metal ions, is allowed by symmetry to interact with the FHOMO-1's of the 2,2′-bipyridine ligands to give the π-in-nature b_{3g} HOMO of the oxo complex (Figure 6a for **6**). The virtual FLUMO+1 of the $Au_2O_2^{2+}$ core, which is derived from the antibonding combination of the gold $5d_{xz}$ AOs with the in-plane p-type AOs of the oxygen atoms, can combine instead with the FHOMOs of the 2,2′-bipyridine ligands to give the σ-in-nature b_{2u} LUMO of the complex (Figure 6b for **6**).

Finally, it is interesting to compare the nature of the LUMOs with the results obtained from the cyclic voltammetry measurements. Indeed, the composition and antibonding nature of this MO clearly explain the irreversible nature of the first reduction process and the nonindependence of the two metal centers. It is noteworthy that the trend of the LUMO energies calculated for **1**−**6** can be compared to the trend of the reduction potentials (Table 3). In fact, although the changes in the thermodynamic parameters involved in the redox process leading to the reduced species have not been taken into account, it can be noted that while the LUMO eigenvalues calculated for **1** and **3** (which featured similar E_{pc} values) were very close to each other, the lowest LUMO eigenvalue was the one calculated for **6** (Table 6). This result indicates that **6** is the most readily reducible complex cation in the series, in agreement with the higher E_{pc} value measured for **6** compared with those recorded for **1**−**5** (Table 3).

Identification of Some Initial Structure–Function Relationships. The relevant inhibition by **1–6** of the growth of A2780 human ovarian carcinoma tumor cells in vitro was described in a previous study.[13] It was found that **6** was the compound producing the strongest inhibition, with an IC_{50} value of ∼1.79 μM; in contrast, the other compounds exhibited less-pronounced cytotoxic action, with IC_{50} values falling in the range 8–26 μM. Relevant IC_{50} values for all six compounds are compiled in Table 7.

In the same study, it was proposed that the cytotoxic effects induced by these binuclear gold(III) compounds are not a consequence of direct DNA binding and damaging (as in the case of classical platinum metallodrugs) but most likely arise from alteration of mitochondrial processes, probably mediated by potent inhibition of the selenoenzyme thioredoxin reductase.[13] The reactions of two representative members of the series, **1** and **6**, with a few proteins considered as appropriate models of "real" biomolecular targets were thus analyzed. Notably, an interesting reactivity, most likely due to the occurrence of redox processes, was detected with proteins such as serum albumin and cytochrome *c*; in particular, **6** was found to manifest a very high reactivity.[13]

The results of the present study further support those observations. In fact, we have clearly shown here that **6** is the compound that most greatly deviates from the "average" chemical behavior within the series in terms of structural

(52) In agreement with the previous observations, the Au−N Wiberg bond indices (see Table S2 in the Supporting Information) decreased only marginally in going from **1** to **6**, while the index related to the interaction between the two O atoms increased slightly.

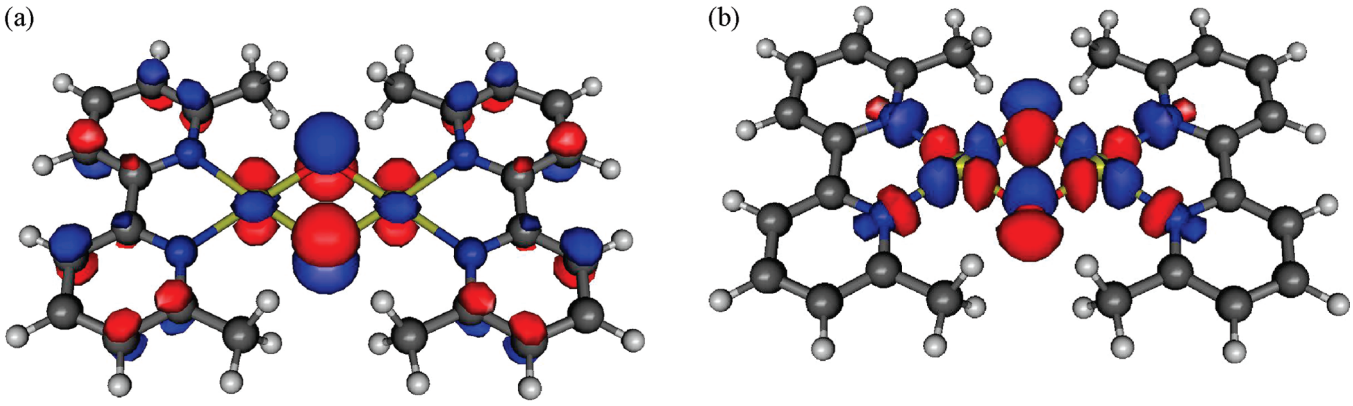

Figure 6. Isosurfaces of the KS (a) b_{3g} HOMO and (b) b_{2u} LUMO calculated for **6** (contour value 0.04 e, point group D_{2h}).

Table 7. IC_{50} Values for Inhibition of A2780[a] Human Ovarian Carcinoma Tumor Cell Growth by the Dinuclear Gold(III) Compounds **1**−**6** Compared with Those for the Mononuclear Precursor **OH1** and Cisplatin (CDDP)

inhibitor	CDDP	**OH1**	**1**	**2**	**3**	**4**	**5**	**6**
$IC_{50}(\mu M)$[b]	2.1 ± 0.2	8.4 ± 0.1	22.8 ± 1.5	12.1 ± 1.5	25.4 ± 2.5	12.7 ± 1.1	11.0 ± 1.5	1.8 ± 0.2

[a] A2780/S cell line. [b] Mean ± SE of three independent experiments performed with quadruplicate cultures at each concentration used.

features, thermal stability, and redox properties. On the other hand, **6** is also the compound that most greatly deviates from the "average" biological behavior, i.e., the compound showing the most relevant antiproliferative effects and the largest reactivity with proteins. In particular, **6** is nearly 10 times more effective than its structural analogues in terms of cytotoxic potency. On the basis of the above arguments, we have attempted to establish some initial structure–function relationships for this family of binuclear gold(III) oxo compounds. It appears that small but significant modifications of the Au_2O_2 diamond core, the common structural motif shared by all of these compounds, may result in higher chemical reactivity and a stronger propensity for the binuclear gold(III) compound to react with biomolecular targets. This higher reactivity correlates well with more-pronounced antiproliferative action. Of particular interest is the positive correlation that probably exists between the oxidizing character and the antiproliferative action, which is in good agreement with previous observations concerning ruthenium compounds.[53]

Overall, these observations, if further supported, can provide the opportunity to design new compounds of this series that bear new and specific structural features (e.g., different kinds of substituents) and might display increased chemical reactivity and enhanced cytotoxic effects. In other words, fine-tuning of the reactivity and biological effects of these metal centers could be achieved.

Conclusions

The exhaustive structural analysis that we have performed on binuclear gold(III) oxo complexes, relying on the availability of high-resolution crystal data, has clearly revealed the existence of a common and well-conserved structural motif comprising the two gold centers, the oxo bridges, and the two bipyridine ligands within a roughly planar arrangement. This common structural motif is largely invariant through the various complexes. Indeed, only modest deviations, caused by the introduction of a variety of substituents on the bipyridine ligand and mainly consisting of increases in the Au···Au and Au−N distances and the N−Au−O angles, were observed among the five crystal structures analyzed. Although very small, these structural changes appeared to be crucial in accounting for the relevant differences observed in the solution behavior, the overall reactivity, and, accordingly, the biological and pharmacological properties of these compounds.

Extensive theoretical calculations based on the DFT approach have been performed on these systems, leading to extremely satisfactory predictions. Notably, the small structural changes evidenced by the crystallographic analysis could be reproduced theoretically with very good accuracy. This result suggests that the observed structural variations are primarily due to electronic features rather than solid-state effects. Moreover, the DFT calculations proved very efficacious in reproducing the order of the experimentally determined reduction potentials.

A direct electronic interaction between the two Au centers of these binuclear complexes was hypothesized and appeared to be supported by the electrochemical results and the short Au···Au distance.

Finally, efforts were made to correlate the main chemical properties of these gold(III) complexes to their antiproliferative actions. Notably, an initial positive correlation has emerged between the oxidizing power and the cytotoxic potency. In particular, we have observed that $[Au_2(\mu\text{-}O)_2(6,6'\text{-}Me_2bipy)_2](PF_6)_2$ (**6**), the compound possessing the most pronounced oxidizing character, exhibits the greatest reactivity with model proteins and the largest cytotoxic effects. Such correlations might be further exploited to design new and more-active gold-based anticancer agents.

Acknowledgment. Ente Cassa di Risparmio di Firenze is gratefully acknowledged for financial support. A.C. acknowl-

(53) Jakupec, M. A.; Reisner, E.; Eichinger, A.; Pongratz, M.; Arion, V. B.; Galanski, M.; Hartinger, C. G.; Keppler, B. K. *J. Med. Chem.* **2005**, *48*, 2831.

edges a grant from AIRC. C.R. gratefully acknowledges CIRCMSB for a one-year fellowship. M.A. thanks CINECA (Consorzio Interuniversitario per il Calcolo Automatico) for computational facilities. For financial support, M.A.C. and G.M. thank the University of Sassari (FAR 2006) and P.Z. thanks the University of Siena (PAR 2007). CRIST (Centro Interdipartimentale di Cristallografia Strutturale, Università di Firenze) is gratefully acknowledged for technical assistance with X-ray data collection.

Supporting Information Available: Figures illustrating stacking interactions in the crystal lattices of *cis*-**3** and *trans*-**5**; a figure and a table comparing selected experimental and calculated bond lengths and angles for **1**; and a table of Wiberg bond indices for **1**, *cis*-**3**, *trans*-**3**, and **6**. This material is available free of charge via the Internet at http://pubs.acs.org. Tables of crystallographic data, positional parameters, isotropic and anisotropic thermal factors, and bond distances and angles in CIF format; all of the DFT-optimized structures in orthogonal Cartesian coordinate format; and Wiberg bond indexes and NBO charges are available from the authors on request.

IC701254S